Overall Electrical Parameters Identification for IPMSMs Using Current Derivative to Avoid Rank Deficiency

Yelong Yu, Xiaoyan Huang, *Member, IEEE*, and Zhaokai Li

***Abstract*—An approach to identify overall electrical parameters for interior permanent magnet synchronous motors (IPMSMs) in steady state is proposed in this article using current derivative, with which the concerns of rank deficiency can be avoided. It is found that the conventional IPMSM models under d-q frame always neglected the pulsewidth modulation (PWM) switching effect of inverter and the quantities in these models are always regarded as constant values in steady state, making it untoward to identify all motor parameters simultaneously. Instead, the switching IPMSM model is built to analyze the details of PWM, and full-rank current derivative functions during zero and active voltage vectors are given, respectively. Without any injected signals, all electrical parameters including *dq*-axis inductance, stator resistance, and permanent magnet flux linkage are able to be figured out in steady state by measuring the phase current derivatives. Simulations and experiments are implemented to validate the proposed approach.**

***Index Terms*—Interior permanent magnet synchronous motors, parameter identification, rank deficiency problem.**

I. Introduction

MOTOR parameters are important for the motor control [1] and condition monitoring [2], [3]. However, the overall parameters including *dq*-axis inductance $L_{d,q}$, stator resistance R, and PM flux linkage ψ_f cannot be easily estimated due to rank deficiency [4], [5] with only two equations under *d-q* frame in steady state. In the literature, some measures have been taken to deal with rank deficiency: 1) to fix some parameters [6], which fails to identify overall parameters; 2) signal injection [7], [8]; 3) under different operations (not steady state) [9]; 4) to estimate parameters in two steps [10], with which initial sensitivity should be addressed [11].

Hence, the aforementioned measures are still unable to identify overall electrical parameters under the strict condition of "*no signal injection, random initial values, and steady operation*".

Manuscript received 13 April 2022; revised 9 July 2022 and 7 August 2022; accepted 24 August 2022. Date of publication 12 September 2022; date of current version 17 February 2023. This work was supported in part by the National Key R&D Program of China under Grant 2019YFE0123500, in part by the Zhejiang Provincial Ten-Thousand-Talent Plan under Grant 2019R52003, and in part by the Liaoning Provincial Natural Science Foundation of China under Grant 2021-KF-24-03. *(Corresponding author: Xiaoyan Huang.)*

The authors are with the Zhejiang University, Hangzhou 310058, China (e-mail: yuyelong@zju.edu.cn; xiaoyanhuang@zju.edu.cn; lzk_zju@zju.edu.cn).

Color versions of one or more figures in this article are available at https://doi.org/10.1109/TIE.2022.3203751.

Digital Object Identifier 10.1109/TIE.2022.3203751

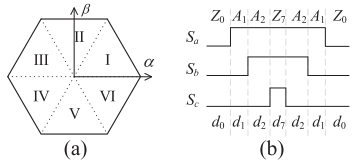

Fig. 1. (a) SVPWM hexagon with six sectors. (b) PWM voltage waveform (sector I) with two active (A_1, A_2) and two zero (Z_0, Z_7) voltage vectors.

Recently, pulsewidth modulation (PWM) switching effect of inverter have been considered for parameters identification [12], with which the stator inductances have been identified [13], [14]. However, the overall parameters identifications for interior permanent magnet synchronous motors (IPMSMs) under the abovementioned strict condition are still missing in the real applications.

In this article, an approach to identify overall parameters for IPMSMs in steady state is proposed using current derivatives. The switching model of IPMSMs is constructed first. Then, the overall parameter identification procedure using the measured current derivative is proposed. Finally simulations and experiments are carried out to verify the proposed approach.

II. Average and Switching Models for IPMSMs

The generalized model for IPMSMs under *d-q* frame is

$$\begin{aligned} u_d &= Ri_d + L_d\frac{di_d}{dt} - \omega_e L_q i_q, \\ u_q &= Ri_q + L_q\frac{di_q}{dt} + \omega_e L_d i_d + \omega_e \psi_f \end{aligned} \tag{1}$$

where $u_{d,q}$ are *dq*-axis voltages; $i_{d,q}$ are *dq*-axis currents; ω_e denotes electrical angular speed. The quantities in (1) are often regarded as constant values in steady state, thus (1) becomes "average" model, which is widely used in motor control and ignores the PWM switching effect. Instead, the switching model considering this effect is constructed here. For the inverter-fed IPMSMs, input voltages are modulated with space vector pulsewidth modulation (SVPWM), as shown in Fig. 1(a), the whole space (hexagon) are divided into six different sectors. In each sector, e.g., sector I, as shown in Fig. 1(b), two active (A_1, A_2) and two zero (Z_0, Z_7) voltage vectors are included in the PWM voltage waveforms.

It can be easily understood that although the fundamental voltages are sinusoidal waveforms, the instantaneous voltages

TABLE I
VOLTAGE VECTORS IN DIFFERENT SECTORS (P.U., WITH THE REFERENCE VOLTAGE VDC)

Area	Vector	S_a	S_b	S_c	$u_{\alpha s}$(p.u.)	$u_{\beta s}$(p.u.)	u_{ds}(p.u.)	u_{qs}(p.u.)
I	A_1	1	0	0	2/3	0	2/3cos(θ_e)	-2/3sin(θ_e)
	A_2	1	1	0	1/3	$\sqrt{3}$/3	2/3cos(θ_e-π/3)	-2/3sin(θ_e-π/3)
II	A_1	0	1	0	-1/3	$\sqrt{3}$/3	2/3cos(θ_e-2π/3)	-2/3sin(θ_e-2π/3)
	A_2	1	1	0	1/3	$\sqrt{3}$/3	2/3cos(θ_e-π/3)	-2/3sin(θ_e-π/3)
III	A_1	0	1	0	-1/3	$\sqrt{3}$/3	2/3cos(θ_e-2π/3)	-2/3sin(θ_e-2π/3)
	A_2	0	1	1	-2/3	0	2/3cos(θ_e-π)	-2/3sin(θ_e-π)
IV	A_1	0	0	1	-1/3	-$\sqrt{3}$/3	2/3cos(θ_e-4π/3)	-2/3sin(θ_e-4π/3)
	A_2	0	1	1	-2/3	0	2/3cos(θ_e-π)	-2/3sin(θ_e-π)
V	A_1	0	0	1	-1/3	-$\sqrt{3}$/3	2/3cos(θ_e-4π/3)	-2/3sin(θ_e-4π/3)
	A_2	1	0	1	1/3	-$\sqrt{3}$/3	2/3cos(θ_e-5π/3)	-2/3sin(θ_e-5π/3)
VI	A_1	1	0	0	2/3	0	2/3cos(θ_e)	-2/3sin(θ_e)
	A_2	1	0	1	1/3	-$\sqrt{3}$/3	2/3cos(θ_e-5π/3)	-2/3sin(θ_e-5π/3)
zero vector	Z_0	0	0	0	0	0	0	0
	Z_7	1	1	1	0	0	0	0

are chopped waves of PWM whose magnitudes are related to dc-link voltage Vdc. Thus, the voltages in switching model under α-β and d-q frames should be expressed as

$$\begin{cases} u_{\alpha s} = \frac{2}{3}(u_a - \frac{1}{2}u_b - \frac{1}{2}u_c) = \frac{1}{3}(u_{ab} + u_{ac}) \\ \quad = \frac{\mathrm{Vdc}}{3}(2S_a - S_b - S_c) \\ u_{\beta s} = \frac{2}{3}(\frac{\sqrt{3}}{2}u_b - \frac{\sqrt{3}}{2}u_c) = \frac{\sqrt{3}}{3}u_{bc} = \frac{\sqrt{3}\mathrm{Vdc}}{3}(S_b - S_c) \end{cases} \tag{2}$$

$$\begin{cases} u_{ds} = u_{\alpha s}\cos\theta_e + u_{\beta s}\sin\theta_e \\ u_{qs} = u_{\beta s}\cos\theta_e - u_{\alpha s}\sin\theta_e \end{cases} \tag{3}$$

where $u_{\alpha s,\beta s}$ are $\alpha\beta$-axis voltages and $u_{ds,qs}$ are dq-axis voltages in the switching model; $u_{a,b,c}$ are phase voltages and $u_{ab,ac,bc}$ are line-to-line voltages under a-b-c frame; $S_{a,b,c}$ refer to the switching states, $S = 1$ means high-side switch is on while $S = 0$ denotes low-side one is on; θ_e is electrical angle. According to (2) and (3), the values of $u_{\alpha s,\beta s}$ and $u_{ds,qs}$ are listed in Table I. Then, the current derivative functions in switching model are given as

$$\begin{aligned} di_{ds}/dt &= u_{ds}/L_d - (Ri_{ds} - \omega_e L_q i_{qs})/L_d \\ di_{qs}/dt &= u_{qs}/L_q - (Ri_{qs} + \omega_e L_d i_{ds} + \omega_e \psi_f)/L_q \end{aligned} \tag{4}$$

where $i_{ds,qs}$ are dq-axis currents in the switching model. Compared to the average model, $u_{ds,qs}$ are not constant anymore; $i_{ds,qs}$ could still be regarded as constant if ignoring the ripples in currents; most important of all, the current derivatives $di_{ds,qs}/dt$ are quite different in the switching model, which could not simply be treated as zero as the average model did.

III. PROPOSED OVERALL PARAMETER IDENTIFICATION

If the current derivatives in (4) are obtained with some measures, they could be used to identify the parameters.

A. Current Derivative Measurement

One of the methods to gain current derivatives is differential circuits, as shown in Fig. 4(a), the differential circuit is attached to the output of Hall sensor, which is applied to measure the currents, then the current derivatives can be easily gained

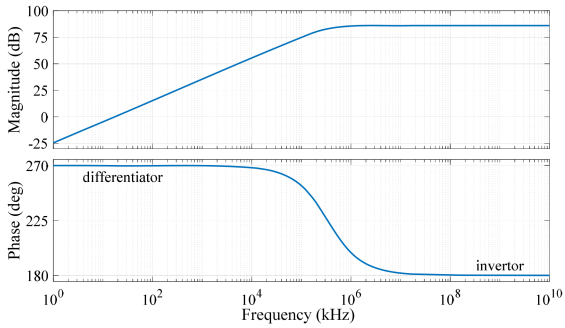

Fig. 2. Frequency response of differential circuit.

$$\begin{aligned} u_{di/dt} = &-R_3C_1\frac{du_{C_1}}{dt} = -R_3C_1\frac{du_i}{dt} \\ &+ \left(\frac{du_i}{dt} - \frac{u_i}{R_1C_1}\right)e^{-t/R_1C_1}. \end{aligned} \tag{5}$$

After the response time of 5–10τ ($\tau = R_1C_1$), the output voltage can reach its steady-state value

$$u_{di/dt} = -R_3C_1\frac{du_i}{dt}. \tag{6}$$

The minimum window for current derivative sampling should be far larger than 10τ, in this case, considering the analog-to-digital converter (ADC) rate, the window must be larger than 2 us. In addition, the available magnitude of output signal must be larger than the noise magnitude $|\xi|$ and cannot exceed the maximum value ADC supports, which can be expressed as

$$|\xi| \ll |u_{di/dt}| < |\mathrm{V_{ADC,max}}| \tag{7}$$

where $\mathrm{V_{ADC,max}}$ denotes the maximum voltage ADC supports. According to (4) and Table I, the current derivatives are related to Vdc and motor parameters, thus, the components of differential circuit should be carefully designed to meet the requirement in (7). Moreover, the frequency response of differential circuit is given in Fig. 2, from which it can be seen that the circuit is performed as differentiator at low frequency ($\leq$100 kHz) while it becomes one kind of phase invertor when the frequency is higher. Obviously, there exists bandwidth for the differential circuit, indicating that it will be challenging to gain the current derivatives with the differential circuit when the switching frequency is very high. In that case, other current derivative sensors such as high-bandwidth Rogowski Coil [15] can be applied for the measurement.

In terms of the accuracy of the differential circuit, all the main components in the circuit should be selected as precise ones, i.e., 0.1% and 1% for resistance and capacitance, respectively. In addition, all the components should have low temperature drifts to guarantee the insensitivity to temperature when measuring the current derivatives.

After measuring the 3-phase current derivatives $di_{as,bs,cs}/dt$ with the differential circuit, $\alpha\beta$-axis and dq-axis current derivatives ($di_{\alpha s,\beta s}/dt$ and $di_{ds,qs}/dt$) could be calculated by

$$di_{\alpha s}/dt = di_{as}/dt,\ di_{\beta s}/dt = (di_{as}/dt + 2di_{bs}/dt)/\sqrt{3} \quad (8)$$

$$\begin{cases} di_{ds}/dt = \cos\theta_e di_{\alpha s}/dt + \sin\theta_e di_{\beta s}/dt \\ \quad +\omega_e(\cos\theta_e i_{\beta s} - \sin\theta_e i_{\alpha s}) \\ = \cos\theta_e di_{\alpha s}/dt + \sin\theta_e di_{\beta s}/dt + \omega_e i_{qs} \\ di_{qs}/dt = \cos\theta_e di_{\beta s}/dt - \sin\theta_e di_{\alpha s}/dt \\ \quad +\omega_e(-\sin\theta_e i_{\beta s} - \cos\theta_e i_{\alpha s}) \\ = \cos\theta_e di_{\beta s}/dt - \sin\theta_e di_{\alpha s}/dt - \omega_e i_{ds}. \end{cases} \quad (9)$$

B. Parameter Identification Approach

For one PWM period, current derivative functions during zero and active vectors in Fig. 1(b) could be written as

$$\text{active}: \begin{aligned} di_{ds\_a}/dt &= u_{ds\_a}/L_d - (Ri_{ds\_a} - \omega_{e\_a} L_q i_{qs\_a})/L_d \\ di_{qs\_a}/dt &= u_{qs\_a}/L_q \\ &\quad - (Ri_{qs\_a} + \omega_{e\_a} L_d i_{ds\_a} + \omega_{e\_a}\psi_f)/L_q \end{aligned} \quad (10)$$

$$\text{zero}: \begin{aligned} di_{ds\_z}/dt &= 0 - (Ri_{ds\_z} - \omega_e L_q i_{qs\_z})/L_d \\ di_{qs\_z}/dt &= 0 - (Ri_{qs\_z} + \omega_e L_d i_{ds\_z} + \omega_{e\_z}\psi_f)/L_q \end{aligned}. \quad (11)$$

Assuming the values of i_{ds}, i_{qs}, and ω_e maintain the same within a PWM period since they are state and continuous variables, which will not be changed sharply like derivatives, there are

$$i_{ds\_a} = i_{ds\_z} = i_{ds},\ i_{qs\_a} = i_{qs\_z} = i_{qs},\ \omega_{e\_a} = \omega_{e\_z} = \omega_e\,. \quad (12)$$

Nevertheless, current derivatives are PWM waveforms and are different during zero and active vectors. Then, the dq-axis inductance could be figured out through

$$L_{d,q} = u_{ds\_a,qs\_a}/(di_{ds\_a,qs\_a}/dt - di_{ds\_z,qs\_z}/dt). \quad (13)$$

After gaining L_d and L_q, R can be also calculated through (11)

$$R = -(L_d di_{ds\_z}/dt - \omega_e L_q i_{qs\_z})/i_{ds\_z}. \quad (14)$$

Finally, ψ_f is able to be obtained also from (11)

$$\psi_f = -(L_q di_{qs\_z}/dt + Ri_{qs\_z} + \omega_e L_d i_{ds\_z})/\omega_e. \quad (15)$$

Hence, it can be seen from (13)–(15) that overall parameters could be identified and there is no rank deficiency problem.

C. Measurement Noise Analysis and RLS

Definitely, there exist noises from the sensors and circuits, hence, in this section recursive least square (RLS) [11] is introduced to identify the parameters with (13)–(15) and the impact of noise has been analyzed. Since all (13)–(15) can be regarded as single input and single output systems, the generalized model is considered and expressed as

$$y_i = wx_i + \xi_i \quad (16)$$

where x, y are the system input and output, respectively; w is the parameter awaiting to be identified; ξ denotes the measurement noise; i means the ith iteration. The key principle of least square is to minimize the cost function J, which represents the mean square error between real output y and the estimated one $\hat{y} = \hat{w}x$

$$\min J = \min \frac{1}{2}\sum_{i=1}^{n}(y_i - \hat{y}_i)^2 = \min \frac{1}{2}\sum_{i=1}^{n}(y_i - \hat{w}x_i)^2 \quad (17)$$

where n denotes the number of samples; $\hat{w}$ is the estimated parameter. Let the gradient of J with respect to $\hat{w}$ be zero in order to obtain the minimum value

$$\frac{\partial J}{\partial \hat{w}} = \sum_{i=1}^{n}(y_i - \hat{w}_i x_i)(-x_i) = 0. \quad (18)$$

Then, the estimated parameter $\hat{w}$ can be figured out in the batch least square (BLS) form

$$\hat{w} = \sum_{i=1}^{n} x_i y_i \Big/ \sum_{i=1}^{n} x_i^2. \quad (19)$$

Since BLS is a standard statistic model, the impact of measurement noise should be analyzed from the perspective of statistic, the measurement of system input, output, and noise can be described as events X, Y, Γ

$$X = [x_1, x_2, \ldots, x_n], Y = [y_1, y_2, \ldots, y_n], \Gamma = [\xi_1, \xi_2, \ldots, \xi_n]. \quad (20)$$

According to (19), the expectation of $\hat{w}$ is calculated by

$$E(\hat{w}) = \frac{E(XY)}{E(X^2)} = \frac{E[X(wX + \Gamma)]}{E(X^2)} = w + \frac{E(X)E(\Gamma)}{E(X^2)} \quad (21)$$

where E is mathematical expectation. With large number of measurement samples, it can be assumed that the noise follow the Gaussian distribution, thus $E(\Gamma) = 0$ and:

$$E(\hat{w}) = w \quad (22)$$

which proves the unbiasedness of parameter estimation $\hat{w}$, indicating that there is no systematic error between $\hat{w}$ and w. However, in some special cases, $E(\Gamma)$ may not be equal to zero especially due to inadequate samples or other reasons, and the unbiasedness might disappear. Fortunately, quantities of bias-compensated algorithms are proposed in other literature [16], [17], [18], since it is not the main work of this letter, these algorithms will not be repeated here. In real applications, there are some points to be remarked in order to eliminate the noise as far as possible: 1) The value of capacitor C_1 cannot be selected too large since it is the main differential element in the circuit. The smaller value of C_1 can prevent the enlargement of noise. 2) The number of measurement samples should be large enough (in this letter, the sample is obtained in each PWM period), according to the abovementioned analyses, the impact of noise would be limited with larger number of samples.

Furthermore, in order to reduce the computational burden, the BLS is transformed to RLS form, let

$$P_n = 1 \Big/ \sum_{i=1}^{n} x_i^2. \quad (23)$$

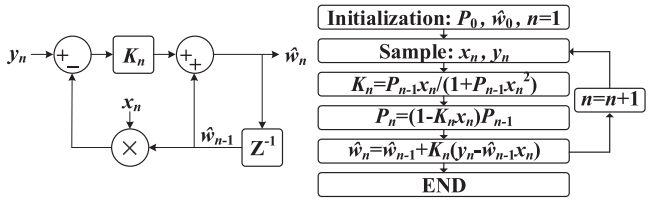

Fig. 3. Block diagram and flowchart of RLS.

TABLE II
RLS SYSTEM FOR MOTOR PARAMETER IDENTIFICATION

Parameter	Input x	Output y
L_d	di_{ds_a}/dt - di_{ds_z}/dt	u_{ds_a}
L_q	di_{qs_a}/dt - di_{qs_z}/dt	u_{qs_a}
R	$-i_{ds\_z}$	$L_d\, di_{ds\_z}/dt$ - $\omega_e L_q\, di_{qs\_z}$
ψ_f	$-\omega_e$	$L_q\, di_{qs\_z}/dt$+Ri_{qs_z}+$\omega_e L_d\, i_{ds\_z}$

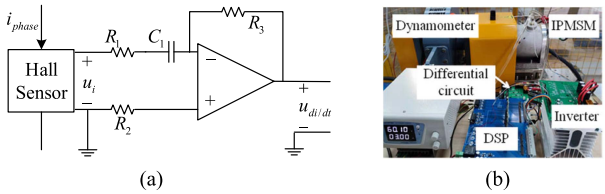

Fig. 4. (a) Differential circuit. (b) Experimental rig.

Substituting (23) into (19), yields

$$\begin{aligned}\hat{w}_n &= P_n \sum_{i=1}^{n} x_i y_i = P_n \left(\sum_{i=1}^{n-1} x_i y_i + x_n y_n \right) \\ &= P_n[\hat{w}_{n-1}(P_n^{-1} - x_n^2) + x_n y_n] \\ &= \hat{w}_{n-1} + P_n x_n (y_n - \hat{w}_{n-1} x_n). \end{aligned} \tag{24}$$

In addition, there are

$$\begin{aligned} K_n &= P_n x_n = P_{n-1} x_n / (1 + P_{n-1} x_n^2) \\ P_n &= (1 - K_n x_n) P_{n-1}. \end{aligned} \tag{25}$$

The quantities of (24) and (25) are all in the recursive form, being easy for the microcontroller units to implement. It should be also noted that RLS can also be regarded as one kind of closed-loop observer, the block diagram and flowchart of RLS can be depicted in Fig. 3 according to (24). The stability of RLS had been proven by the passivity theorem in [19] and [20].

Applying the RLS, the motor parameters can be finally identified with (13)–(15), the RLS system for all four motor parameters are listed in Table II.

IV. SIMULATIONS AND EXPERIMENTS

To verify the proposed approach of parameter identification, the simulations and experiments are implemented. The simulation is based on MATLAB/Simulink, while the experimental rig including IPMSM prototype and its driven inverter, DSP (TI F28379) board and differential circuit is photographed in Fig. 4(b). The parameters of the tested IPMSM, inverter and differential circuit are listed in Table III. The IPMSM is controlled with maximum torque per ampere algorithm.

TABLE III
PARAMETERS OF TESTED IPMSM, INVERTER, AND DIFFERENTIAL CIRCUIT

Phase	Poles	Slots	Winding	Rated speed	Rated current	Vdc	Switching frequency
3	4	24	Star	1200 r/min	5 A	60 V	10 kHz
R	Ld	Lq	ψ_f	R_1	R_2	R_3	C_1
0.1Ω	0.60 mH	0.91 mH	0.058 Wb	10 Ω (0.1%)	1 kΩ (0.1%)	200 kΩ (0.1%)	47 pF (1%)

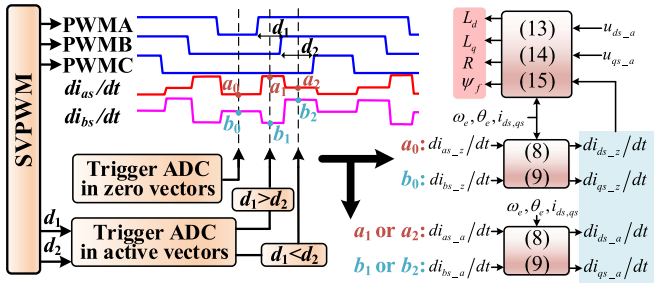

Fig. 5. Scheme of hardware and software implementation.

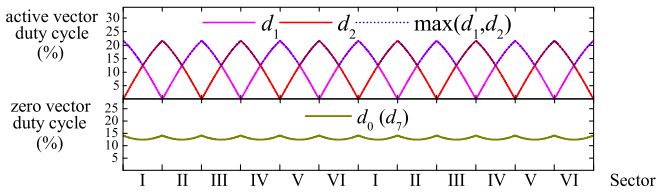

Fig. 6. Duty cycle of active and zero vectors in different sectors of SVPWM hexagon.

A. Implementation Procedure

The hardware and software implementation procedure is outlined in Fig. 5, ADC is firstly triggered to sample the *ab*-axis current derivatives during zero vectors (di_{as_z}/dt, di_{bs_z}/dt). Generally the *ab*-axis currents (i_{as}, i_{bs}) could be also sampled at this moment for current loop control. Subsequently, ADC will be trigger again by PWM rising edge (a delay time will often be inserted to reject transient switching disturbance) to measure current derivatives during active vectors (di_{as_a}/dt, di_{bs_a}/dt). The window selection of active vectors depends on the width of duty cycles, the waveforms of the two active vectors duty cycles (see d_1 and d_2 in Fig. 1) are depicted in Fig. 6. The active vectors with larger duty cycle, referring to max(d_1,d_2), are chosen to be the sampling window in order to guarantee adequate time for current derivative measurement. All the measured current derivatives under *a-b-c* frame are transformed to the ones under *d-q* frame through (8), (9), and finally, $L_{d,q}$, R, and ψ_f are identified with (13)–(15). At low speed and light load, it may become challenging since both of the windows (d_1 and d_2) are narrow, which indeed is similar to the issues regarding single-shunt current sensing for the motor control [21], [22].

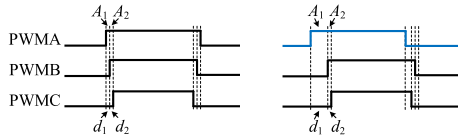

Fig. 7. Technique of PWM shifting at low speed and light load.

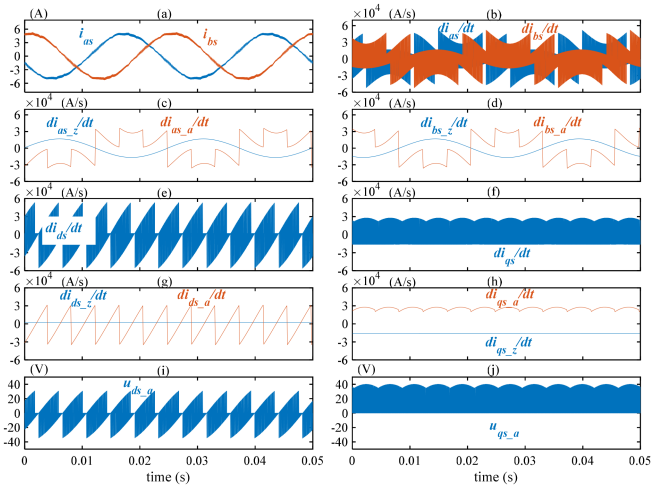

Fig. 8. Simulated waveforms of currents and derivatives, voltages.

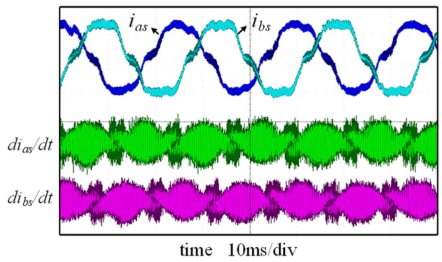

Fig. 9. Experimental waveforms of currents and derivatives.

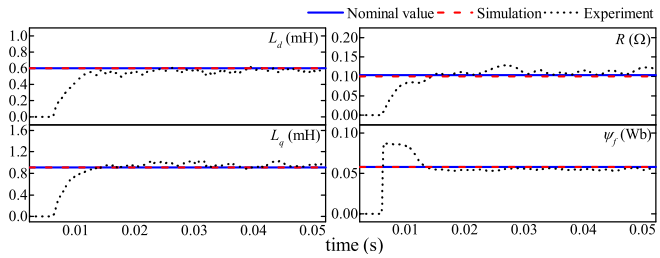

Fig. 10. Results of overall parameter identification.

In this case, the technique of PWM shifting shown in Fig. 7 can be applied to obtain adequate window for sampling, and the duty cycles for all the PWMs have to be preserved.

B. Results in Simulations and Experiments

The simulated *ab*-axis currents with switching ripples (i_{as},i_{bs}) are shown in Fig. 8(a), as mentioned in Section II, the fundamental components of $i_{as,bs}$ are still sinusoids, however, their derivatives $di_{as,bs}/dt$ are not sinusoids but chopped waves in Fig. 8(b). The sampling waveforms of current derivatives during zero and active vectors are shown in Fig. 8(c) and (d), which actually could be regarded as the envelopes of real-time current derivative waveforms in Fig. 8(b). Similarly, the waveforms of current derivatives and their sampling data under *d*-*q* frame are presented in Fig. 8(e)–(h). It should be remarked that after applying the low pass filter to di_{ds}/dt and di_{qs}/dt, the high-frequency harmonics will be eliminated and the dc components of di_{ds}/dt and di_{qs}/dt are zero in steady state as the same as those in the average model (di_d/dt and di_q/dt). The values of u_{ds} and u_{qs}, which are listed in Table I are also given in Fig. 8(i) and (j).

In addition, the experimental waveforms of currents and their derivatives from the differential circuit are shown in Fig. 9. Implementing the procedure of parameter identification which is demonstrated in Section IV-A, the overall parameters can be figured out, which is depicted in Fig. 10. The initial values of estimated parameters are all set as zero in the experiments, after the convergence time (≈0.01 s), the estimated values could be adjacent to their nominal values. The errors in the parameter identification are mainly caused by the parasitic parameters in the circuit, ADC errors and other possible reasons. Since the parameter identifications are implemented in recursive form, the computational burden is very low, the implementation time is less than 10 us during each RLS iteration.

V. Conclusion

This article proposed an overall parameters identification for IPMSMs. Considering the details of PWM, the switching model was constructed, with which the current derivative functions during active and zero voltage vectors were derived. The approach of full-rank parameters identification was illustrated with the help of RLS and measured current derivatives from differential circuits. Finally, the hardware and software implementation procedure were introduced and the results in simulations and experiments can validate the proposed approach. Obviously, the approach in this article was able to overcome the rank-deficiency problem and identify the overall electrical parameters in steady state without any signal injection. However, more efforts were still needed to improve the problems of measurement noise and very high switching frequency in the future real-world applications.

References

[1] N. Jabbour and C. Mademlis, "Online parameters estimation and autotuning of a discrete-time model predictive speed controller for induction motor drives," *IEEE Trans. Power Electron.*, vol. 34, no. 2, pp. 1548–1559, Feb. 2019.

[2] J. Sun, C. Li, Z. Zheng, K. Wang, and Y. Li, "Online estimation of per-phase stator resistance based on DC-Signal injection for condition monitoring in multiphase drives," *IEEE Trans. Ind. Electron.*, vol. 69, no. 3, pp. 2227–2239, Mar. 2022.

[3] D. Reigosa, D. Fernández, M. Martínez, Y. Park, S. B. Lee, and F. Briz, "Permanent magnet synchronous machine non-uniform demagnetization detection using zero-sequence magnetic field density," *IEEE Trans. Ind. Appl.*, vol. 55, no. 4, pp. 3823–3833, Jul./Aug. 2019.

[4] Z. Q. Zhu, D. Liang, and K. Liu, "Online parameter estimation for permanent magnet synchronous machines: An overview," *IEEE Access*, vol. 9, pp. 59059–59084, 2021.
[5] P. Vaclavek, P. Blaha, and I. Herman, "AC drive observability analysis," *IEEE Trans. Ind. Electron.*, vol. 60, no. 8, pp. 3047–3059, Aug. 2013.
[6] Y. Shi, K. Sun, L. Huang, and Y. Li, "Online identification of permanent magnet flux based on extended kalman filter for IPMSM drive with position sensorless control," *IEEE Trans. Ind. Electron.*, vol. 59, no. 11, pp. 4169–4178, Nov. 2012.
[7] S. A. Odhano, R. Bojoi, Ş. G. Roşu, and A. Tenconi, "Identification of the magnetic model of permanent-magnet synchronous machines using DC-Biased low-frequency AC signal injection," *IEEE Trans. Ind. Appl.*, vol. 51, no. 4, pp. 3208–3215, Jul./Aug. 2015.
[8] G. Feng, C. Lai, K. Mukherjee, and N. C. Kar, "Current injection-based online parameter and VSI nonlinearity estimation for PMSM drives using current and voltage DC components," *IEEE Trans. Transp. Electrific.*, vol. 2, no. 2, pp. 119–128, Jun. 2016.
[9] K. Liu, Z. Q. Zhu, and D. A. Stone, "Parameter estimation for condition monitoring of PMSM stator winding and rotor permanent magnets," *IEEE Trans. Ind. Electron.*, vol. 60, no. 12, pp. 5902–5913, Dec. 2013.
[10] D. Q. Dang, M. S. Rafaq, H. H. Choi, and J. Jung, "Online parameter estimation technique for adaptive control applications of interior PM synchronous motor drives," *IEEE Trans. Ind. Electron.*, vol. 63, no. 3, pp. 1438–1449, Mar. 2016.
[11] Y. Yu et al., "Full parameter estimation for permanent magnet synchronous motors," *IEEE Trans. Ind. Electron.*, vol. 69, no. 5, pp. 4376–4386, May 2022.
[12] K. Choi, Y. Kim, K.-S. Kim, and S.-K. Kim, "Using the stator current ripple model for real-time estimation of full parameters of a permanent magnet synchronous motor," *IEEE Access*, vol. 7, pp. 33369–33379, 2019.
[13] J. Zhang, F. Peng, Y. Huang, Y. Yao, and Z. Zhu, "Online inductance identification using PWM current ripple for position sensorless drive of high-speed SPMSM," *IEEE Trans. Ind. Electron.*, vol. 69, no. 12, pp. 12426–12436, Dec. 2022.
[14] M. X. Bui, M. Faz Rahman, D. Guan, and D. Xiao, "A new and fast method for On-line estimation of d and q axes inductances of interior permanent magnet synchronous machines using measurements of current derivatives and inverter DC-Bus voltage," *IEEE Trans. Ind. Electron.*, vol. 66, no. 10, pp. 7488–7497, Oct. 2019.
[15] A. Mingotti, L. Peretto, and R. Tinarelli, "A smart frequency domain-based modeling procedure of rogowski coil for power systems applications," *IEEE Trans. Instrum. Meas.*, vol. 69, no. 9, pp. 6748–6755, Sep. 2020.
[16] R. Arablouei, K. Doğançay, and T. Adalı, "Unbiased recursive least-squares estimation utilizing dichotomous coordinate-descent iterations," *IEEE Trans. Signal Process.*, vol. 62, no. 11, pp. 2973–2983, Jun. 2014.
[17] S. M. Jung and P. Park, "Stabilization of a bias-compensated normalized least-mean-square algorithm for noisy inputs," *IEEE Trans. Signal Process.*, vol. 65, no. 11, pp. 2949–2961, Jun. 2017.
[18] C. Liu and H. Zhao, "Efficient DOA estimation method using bias-compensated adaptive filtering," *IEEE Trans. Veh. Technol.*, vol. 69, no. 11, pp. 13087–13097, Nov. 2020.
[19] K. Hidakal, "Novel RLS algorithm with internal model and its stability margin," in *Proc. IEEE 41st SICE Annu. Conf.*, 2002, vol. 2, pp. 1239–1240.
[20] K. J. Astrom and B. Wittenmark, *Adaptive Control*. Reading, MA, USA: Addison-Wesley, 1995.
[21] Y. Gu, F. Ni, D. Yang, and H. Liu, "Switching-State phase shift method for three-phase-current reconstruction with a single DC-Link current sensor," *IEEE Trans. Ind. Electron.*, vol. 58, no. 11, pp. 5186–5194, Nov. 2011.
[22] J. Ha, "Voltage injection method for three-phase current reconstruction in PWM inverters using a single sensor," *IEEE Trans. Power Electron.*, vol. 24, no. 3, pp. 767–775, Mar. 2009.